# Phenomenological Model-Based Analysis of Lithium Batteries: Discharge, Charge, Relaxation Times Studies, and Cycles Analysis

**Eduardo R. Henquín and Pio A. Aguirre**
Instituto de Desarrollo y Diseño (INGAR), Consejo Nacional de Investigaciones Científicas y Técnicas (CONICET), Avellaneda 3657, S3002GJC Santa Fe, Argentina

*DOI 10.1002/aic.14618*
*Published online September 16, 2014 in Wiley Online Library (wileyonlinelibrary.com)*

*The operation of lithium ion batteries in discharge and charge processes is addressed. A simple phenomenological model is developed to predict all variables values. A set of algebraic and differential equations is derived taking into account salt and lithium balances in electrodes, in the separator, and in particles. Balances are developed for finite volumes and appropriate average values of several variables such as concentrations, current densities, and electrochemical reaction rates are introduced. Definitions of current densities as volume fraction functions are critical issues in the computations. Experimental values taken from the literature for discharge processes are predicted very accurately. Constant salt concentration in the separator can be assumed and consequently, the model can be analytically solved. Charge and discharge times, initial cell capacity, lost capacity, and relaxation times are easily estimated from simple equations and cell parameters. The limiting processes taking place during cell discharge can be determined. Energy efficiency and capacity usage are quantified for cycles.* © 2014 American Institute of Chemical Engineers *AIChE J*, 61: 90–102, 2015
*Keywords: lithium ion batteries, cyclic processes, simplified mathematical modeling, capacity estimation, relaxation time*

## Introduction

Power supply systems based on the use of Lithium ion batteries are potentially attractive for achieving reductions in operating costs, emissions of greenhouse gases, and oil consumption in both vehicle transportation and stationary applications. These systems offer a very good ratio of delivered energy density in relation to their size and have greater efficiency in comparison with other energy storage devices, which allows for the use of larger amounts of charge–discharge cycles. They also lack the undesirable memory effects, preserving its capacity even with incomplete charge.[1]

However, the net effect of these systems depends critically on the design of an energy-consuming device, the technical design of the battery, the temporal pattern of power delivery, charge times, and system capabilities for charging the batteries.

Energy demand profiles required by a technological application for being operated could be interpreted as charge, discharge, and switched off sequences imposed upon the battery. If these sequences are identically repeated in continuous periods, a cyclic process is configured. It is characterized by repeating a pattern over time, in which the involved variables take again those values they had at the beginning of the cycle. Most current technological applications for rechargeable batteries are designed to work on cyclic processes. Many authors have paid attention to this area. Thus, in Ref. 2, optimal charge pattern is studied as a function of the timing and rate in which a plug-in hybrid electric vehicle obtained energy from the power grid. A multiobjective optimization algorithm was used to minimize the total cost of fuel and electricity. In Ref. 3, authors focus the attention on petroleum consumption and greenhouse gases emission problem. The optimization problem includes statistical terms such as: distances between charges, power patterns imposed by different drivers, distribution of vehicle miles traveled per day, vehicle performance models, battery degradation as a function of discharge depth, and so forth. Fuel consumption, lifecycle greenhouse gases and lifecycle cost are analyzed. In Ref. 4, thermal effect and capacity loss in both electrodes are modeled taking into account solid electrolyte interface formation, and solved using finite element method with MATLAB and COMSOL.

Some authors have addressed the issue of energy integration between generators and storage devices for electric power systems working on charge and discharge cycles. In Ref. 5, the design, modeling, and operational analysis of an integrated energy network is investigated. The energy system operates with a wind turbine, a photovoltaic panel, and solid oxide fuel cell. In Ref. 6, microgeneration systems are analyzed, which are composed of a Stirling engine for supplying heat and power, and a lithium-ion battery used to feed a typical Canadian house. Two different kinds of electrode materials are studied through a simulation model.

Physicochemical phenomena occur in short time periods when batteries are operated in cycles. These phenomena

Correspondence concerning this article should be addressed to E. R. Henquín at ehenquin@santafe-conicet.gov.ar.

need to be properly explained. Hence, it is desirable to have prediction models that account for the phenomenological description of lithium ion batteries integrated with an energy consumption system.[7] As regards phenomenological aspects, it becomes necessary the development of mathematical models that describe all diffusion stages, transport, and electrochemical reactions in solid and electrolyte. These steps were well described in Ref. 8, for the couple $Li_xC_6$ | $Li_yMn_2O_4$. Two different spatial subdomains—cell length and particle radius—and a temporal domain were proposed for the partial differential equations model.

Under these circumstances, many authors have studied procedures to facilitate the resolution of this set of equations or decrease computing time. Thus, in Ref. 9, a method for initialization the resolution of differential equation is presented. In Ref. 10, the results of a two-dimensional constant current rigorous model for calculating charge and discharge performance of a unit cell are compared against those of two simplified models. The authors of Ref. 11 simplify the resolution of the system of equations by replacing the concentration profile of the particles by empirical polynomial expressions. In Ref. 12, a simplified model of particle diffusion is presented. A one-dimensional mathematical model that describes performance of a 6-Ah battery used in hybrid vehicles is presented in Ref. 13 by applying the finite element method for approximating lithium diffusion in electrode particles. In Ref. 14, a reformulated model with mathematical techniques and incorporation of simplifications to speed up its resolution is presented. In Ref. 15, the authors compare performance of different previously published simplified methods. The authors of Ref. 16 show an approximate model based on polynomials of second, third, and fourth degree in order to describe the concentration profile in spherical electrode particles. An overview of the mathematical procedures and the software used to model charge and discharge of these batteries is presented in Ref. 17. In Ref. 18, results from another mathematical reformulation are compared with those arising from finite difference scheme. Another important factor in the design of these units is the generation of heat and its consequences in the mathematical modeling.[19,20]

Many authors have made contributions in order to simplify the pose and the resolution of these systems of equations, many procedures for obtaining an algebraic or semialgebraic models, some of which are cited in Ref. 21. Other authors proposed simplified mathematical models based on equivalent circuits to represent charge and discharge cycles of lithium-ion batteries in a short time period. Thereby, in Ref. 22, the author shows a Simulink model regarding the electrochemical and thermal properties to simulate different cell types for an electric drive system. The model is based on an equivalent circuit diagram. A similar approach, in terms of representing the battery as a set of resistors and capacitors, can be consulted at Ref. 23.

Despite the effort put into developing accurate models that can be solved quickly, there is a lack of predictive phenomenological models that can be solved analytically, and with physical and phenomenological bases.

As this work aims at the analysis of system operating in discharge, charge, and cyclic processes, accurate and phenomenological simplified models that account for all the relevant variables are needed. The analysis of charge and discharge processes involve the following aspects of interest: cell potential drop analysis, cell capacity estimation, loss of cell capacity, energy efficiency, reversible and irreversible cell work, and relaxation times[24] in cyclic operation. As it will be seen, the models developed in this work are able to predict and compute all these aspects. The article is organized in the following sections: Currents and potential models; Mass balances for Lithium and salt in each compartment and particle; Simplified models development; Comparison between models; Model validation; Capacity and relaxation times computation; and energy efficiency in charge and discharge processes.

**Table 1. Design Adjustable Parameters**

| Parameter | | Anode: $Li_xC_6$ | Cathode: $Li_yMn_2O_4$ | Separator |
|---|---|---|---|---|
| $\varepsilon_l$ | | 0.357 | 0.444 | 0.724 |
| $\varepsilon_p$ | | 0.146 | 0.186 | 0.276 |
| $\varepsilon_f$ | | 0.026 | 0.073 | |
| $L$ (cm) | Cell 1 | 0.01 | 0.0174 | 0.0052 |
| | Cell 2 | 0.0128 | 0.019 | 0.0076 |
| $\gamma_\kappa$ | Cell 1 | 3 | 3 | |
| | Cell 2 | 1.5 | 1.5 | |
| $D_s$ ($cm^2\ s^{-1}$) | | $3.9 \times 10^{-10}$ | $1.0 \times 10^{-9}$ | |
| $\sigma_0$ ($S\ cm^{-1}$) | | 1.0 | 0.038 | |
| $k$ ($A\ cm^{2.5}\ mol^{-1.5}$) | | 0.18793 | 0.20803 | |
| $R_s$ (cm) | | 0.00125 | 0.00085 | |
| $\gamma_\sigma$ | | 1 | 1.5 | |
| $\gamma_D$ | | 3 | 3 | |
| $C_s^{max}$ ($mol\ cm^{-3}$) | | 0.02639 | 0.02286 | |
| $C_s^0$($mol\ cm^{-3}$) | Cell 1 | 0.01487 | 0.0039 | |
| | Cell 2 | 0.01412 | 0.0035 | |
| $C_e^0$ ($mol\ cm^{-3}$) | Cell 1 | | 0.002 | |
| | Cell 2 | | 0.001 | |
| $D_e$ ($cm^2\ s^{-1}$) | Cell 1 | | $1.51 \times 10^{-6}$ | |
| | Cell 2 | | $2.40 \times 10^{-6}$ | |

## Currents and Potentials Model Equations

The lithium-ion battery modeled in this article consists of a negative electrode (anode) of carbon particles and a positive electrode (cathode) of manganese oxide particles. The models developed in this article will be validated with experimental determinations arising from two different cells published in Ref. 8. Adjustable physicochemical parameters for each electrode and adjustable design parameters for the entire cell were collected from the same article and are shown in Table 1.

To model the ohmics drop into the cell, solid and electrolyte phase in anode, cathode, and separator, the current in each phase must be computed. In solid phase, current is maximum on the collectors and minimum (zero) on the separator. In this work, the average current density value is computed from the following equation

$$i_s^i\ a_{tr.s}^i = \frac{i_{app}}{2}\ a_t, \quad \text{then } i_s^i = \frac{i_{app}}{2\ \left(\varepsilon_s^i + \varepsilon_f^i\right)} \tag{1}$$

and the solid phase cross-sectional area is calculated as

$$a_{tr.s}^i = a_t\left(\varepsilon_s^i + \varepsilon_f^i\right) \tag{2}$$

where $i_{app}$ is the total current density applied on the current collectors of the cell and $i_s$ represents the average current density in solid phase. Meanwhile, superscript i indicates anode or cathode, and $a_t$ is the cross-sectional area of the cell.

By contrast, the minimum current density in solution phase is given on the currents collectors and the highest on

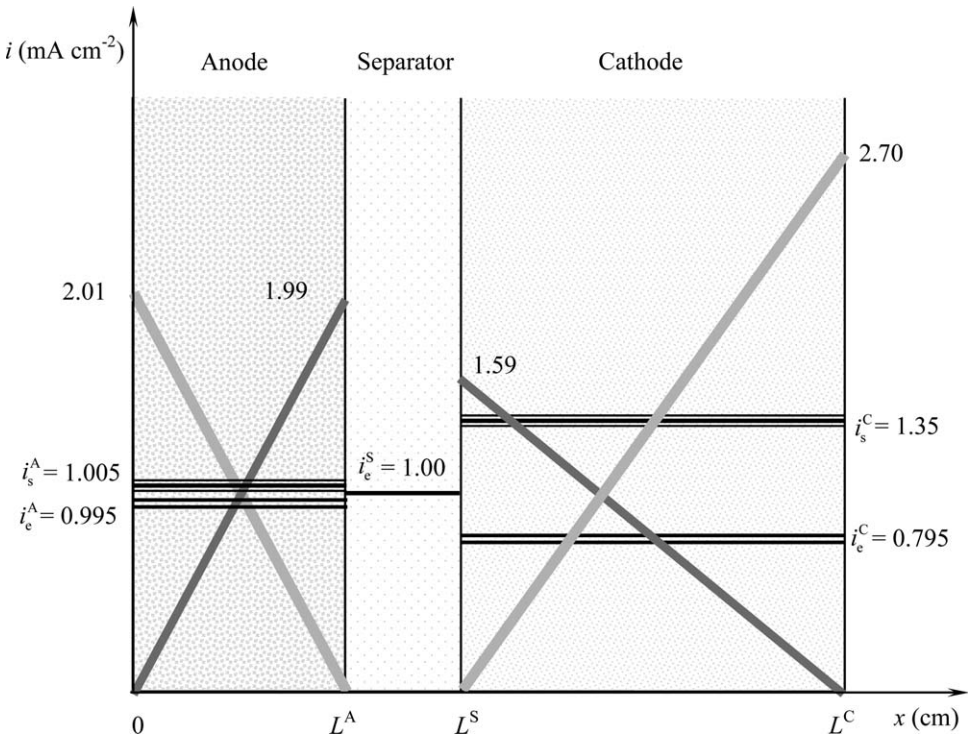


**Figure 1. Relative values of current densities inside the battery.**

**$i_{app} = 1$ mA cm$^{-2}$. (▬): electrolyte current density on electrodes. (▬): solid current density on electrodes. (▬): electrolyte current density on separator. (▬): average electrolyte current density on electrodes. (▬): average solid current density on electrodes.**

the limit with the separator. Taking into account the average of these two values

$$i_e^i \; a_{tr.e}^i = \frac{i_{app}}{2} a_t, \;\; \text{as a consequence} \;\; i_e^i = \frac{i_{app}}{2\left(\varepsilon_l^i + \varepsilon_p^i\right)} \tag{3}$$

where electrolyte phase cross-sectional area in each compartment can be represented as follows

$$a_{tr.e}^i = a_t\left(\varepsilon_l^i + \varepsilon_p^i\right) \tag{4}$$

As it can be seen, Eqs. 1–4 take into account the volumetric fractions of solid and solution phase of each electrode, respectively. There is no solid and conductive filler in the separator. Hence, it is not necessary to calculate the average value of the current density. The electrolyte phase current in the separator is modeled as

$$i_e^S \; a_{tr.e}^i = i_{app}\, a_t, \text{then} \; i_e^S = \frac{i_{app}}{\left(\varepsilon_l^S + \varepsilon_p^S\right)}; \; \text{then} \; i_e^S = i_{app} \tag{5}$$

Adding Eqs. 1 and 3

$$i_{app} \; a_t = i_s^i \; a_{tr.s}^i + i_e^i \; a_{tr.e}^i \tag{6}$$

Even though Eq. 6 was derived for average current values, it is also valid for any position into the battery. As it can be seen, the areas through which ions circulate are different from the areas through which the current flows in solid phase, and thus they cannot be canceled. According to Eq. 6 and using the design adjustable parameters summarized in Table 1, Figure 1 is sketched. The relative values of the current densities are shown for each battery compartment and for all the phases, considering that the applied current density is unitary. It should be noted that extreme values of the linear profile are exact, while interior points are linearly depicted as graphical approximation. Average current densities vary according to phase and compartment.

Potential drop in the electrolyte phase is well known and can be written for the anode as

$$i_e^A = -\kappa_{eff}^A \; \nabla\phi_e^A + \frac{\kappa_{eff}^A \; R \; T}{F}\left(1 + \frac{\partial \ln f_{\pm}}{\partial \ln C_e^A}\right)\left(1 - t_+^o\right) \; \nabla \ln C_e^A \tag{7}$$

In this article, a discretized form of Eq. 7 will be used. To compute the concentration gradient, twice the concentration difference between the middle of the compartment and the limit with the separator is considered. In this manner, a lineal model is applied. Logarithm is discretized with the average concentration of the compartment. Potential gradient of the electrolyte phase will be replaced by the quotient between the potential difference between the ends of the compartment under consideration (right side minus left side) and the thickness of the compartment. Using these considerations, the potential drop in electrolyte phase for anode is expressed

$$\Delta\phi_e^A = -\frac{i_e^A \; L^A}{\kappa_{eff}^A} + \frac{R \; T}{F}\left(1 - t_+^o\right) 2 \frac{\left(C_e^A - C_e^{A,S}\right)}{C_e^A} \tag{8}$$

being $C_e^A$ the average salt concentration in electrolyte of the anode, $C_e^{A,S}$ the concentration of salt at the boundary anode/separator, $\Delta\phi_e^A$ is the difference between the potential on the right side of the anode and the potential on the left side of the anode.

On a similar basis, these equations can be applied to the cathode and the separator.

**Table 2. Parameters for the Two Different Electrolyte Mixture, According to Eq. 10**

| Parameter | Cell 1. 1:2 v/v Mixture of Ethylene Carbonate and Dimethyl Carbonate | Cell 2. 2:1 v/v Mixture of Ethylene Carbonate and Dimethyl Carbonate |
|---|---|---|
| K0 | 243.2 | 289.2 |
| K1 | 1250 | 1110 |
| K2 | 16.2 | 500 |
| K3 | 0.23 | 0.14 |
| K4 | 370 | 355 |

Effective conductivity in electrolyte phase $\kappa^{i}_{eff}$ is expressed as a function of conductivity of the liquid/salt/polymer system as

$$\kappa^{i}_{eff}=\kappa^{i}_{o}\left(\varepsilon^{i}_{l}+\varepsilon^{i}_{p}\right)^{\gamma_{\kappa,i}} \tag{9}$$

In Doyle et al.,[8] conductivity of this system is related with concentration as a fourth-degree polynomial for two different electrolyte mixtures: Cell 1 1:2 v/v mixture of ethylene carbonate and dimethyl carbonate and Cell 2 2:1 v/v mixture of ethylene carbonate and dimethyl carbonate. In this work, functionality proposed in Ref. 25 is adapted

$$\kappa^{i}_{o}=\left[\frac{\left(1+K0\ C^{i}_{e}\ \right)^{2}}{\left(1-K1\ C^{i}_{e}\ \right)^{2}+\left(1+K2\ C^{i}_{e}\right)^{2}+K3}\right]\frac{1}{K4} \tag{10}$$

Table 2 summarizes the parameter for both batteries. In Figure 2, a comparison between experimental points and polynomial expressions used in Ref. 8 and the curves used in this article according to Eq. 10 are shown.

The potential drop in solid phase can be expressed as

$$\Delta\phi^{i}_{s}=\frac{i^{i}_{s}\ L^{i}}{\sigma^{i}_{eff}} \tag{11}$$

where $\Delta\phi^{i}_{s}$ means the potential difference between the right and the left side of the compartment i. Effective conductivity $\sigma^{i}_{eff}$ can be written as a function of conductivity of the pure phase, as it was similarly published in Ref. 8

$$\sigma^{i}_{eff}=\sigma^{i}_{o}\left(\varepsilon^{i}_{s}+\varepsilon^{i}_{f}\right)^{\gamma_{\sigma,i}} \tag{12}$$

Electrochemical reaction velocity is related to the average applied current density value in either anode or cathode, taking into account that it is carried out on the particles surface in each electrode. Hence

$$i_{app}\ a_{t}=\ j^{i}\ F\ a^{i}_{e/s},\ \text{then}\ j^{i}=\frac{i_{app}}{\varepsilon^{i}_{s}\ F\ L^{i}}\frac{v^{i}_{s}}{a^{i}_{s}} \tag{13}$$

The contact area between spherical particles and electrolyte phase is

$$a^{i}_{e/s}=v^{i}_{s}\frac{3}{R^{i}_{s}} \tag{14}$$

Overpotential is calculated considering a Butler–Volmer kinetic for electrodes reactions being $\alpha a = \alpha b$. Exchange current density is expressed as usual in the literature

$$\eta^{i}=\frac{R\ T}{0.5\ F}\sinh^{-1}\left(\frac{j^{i}\ F}{2\ j0^{i}}\right),\ \text{with}\ j0^{i}=k^{i}\left[C^{i}_{surf}\ C^{i}_{e}\left(C^{i}_{max}-C^{i}_{surf}\right)\right]^{0.5} \tag{15}$$

where $C_{surf}$ refers to the value of concentration in the particle surface. Open circuit potentials vs. state of charge on both electrodes, $U^{i}_{\theta}$, are represented by the functionality informed in Ref. 8, with

$$\theta^{i}=C^{i}_{surf}/C^{i}_{max} \tag{16}$$

Taking into account all the above stated potential drops, cell potential can be expressed as follows

$$U_{cell}=U^{C}_{\theta}-U^{A}_{\theta}-\eta^{C}-\eta^{A}-\Delta\phi^{C}_{s}-\Delta\phi^{A}_{s}-\Delta\phi^{C}_{e}-\Delta\phi^{A}_{e}-\Delta\phi^{S}_{e} \tag{17}$$

It should be recalled that $\Delta$ refers to the difference between the potentials of the right minus potentials of the left of the corresponding phases.

Changes over time of salt concentration in electrolytes and lithium concentration in particles must be known for solving Eq. 17. Different assumptions about both electrolyte and solid electrodes will be presented according to different approaches. Results obtained from these alternatives will be compared.

## Salt Mass Balances in Electrolyte Compartments

Lithium salt flows from the anode to the cathode in the discharge process of the battery. A schematic diagram of salt flows, and salt concentration profile is sketched in Figure 3. In this article, average salt concentration in the electrolyte phase, $C^{i}_{e}$, is the variable used in mass balances. Furthermore, it is assumed that local salt concentration takes the value of average concentration $C^{i}_{e}$ in a point corresponding to the middle volume of the domain.

Salt mass balance for electrolyte phase in the anode results

$$v^{A}_{e}\ \frac{dC^{A}_{e}}{dt}=\ j^{A}\left(1-t^{0}_{+}\right)a^{A}_{e/s}-N^{A}_{diff} \tag{18}$$

where variation of salt moles in the anode comes from the electrochemical reaction and lithium salt flow out of the

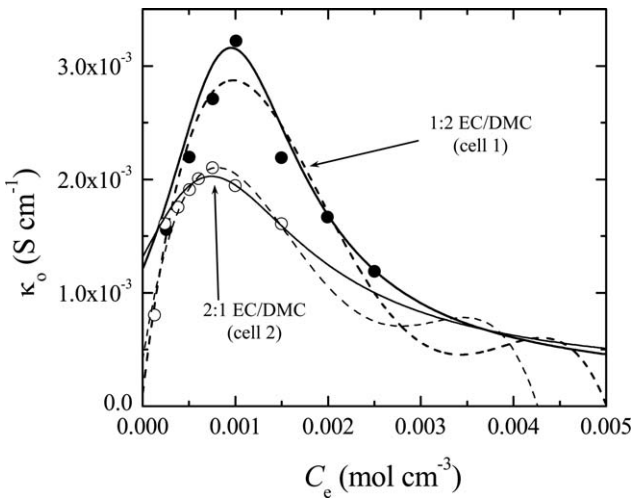


**Figure 2. Conductivity of the electrolyte, as a function of the salt concentration.**

**Dots: experimental points according to Ref. 8. (•): 1:2 v/v mixture of ethylene carbonate and dimethyl carbonate (EC/DMC). (○): 2:1 v/v mixture of EC/DMC. Dash lines: Correlation according to Ref. 8. Continues line: Correlation of this article.**

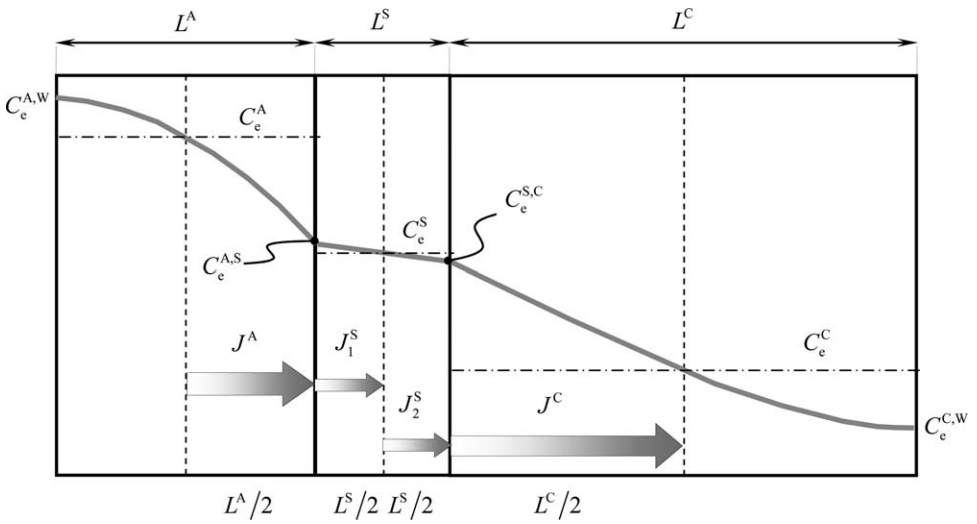


**Figure 3. Concentration gradient and salt flow on the electrolyte phase.**

compartment. As it can be seen, Eq. 18 corresponds to an average in the length coordinate of equation [A-1] described in Ref. 8, considering the gradient of transport number as negligible. By similarity, lithium salt mass balance in the cathode can be expressed by

$$v_e^C \frac{dC_e^C}{dt} = -j^C\left(1-t_+^o\right)a_{e/s}^C + N_{diff}^C \tag{19}$$

Lithium salt mass balance in the separator takes into account the flow between both, anode and cathode

$$v_e^S \frac{dC_e^S}{dt} = N_{diff}^A - N_{diff}^C \tag{20}$$

being

$$N_{diff}^i = J^i a_{tr.e}^i, \text{ with } J^i = -D\frac{dC^i}{dx} \tag{21}$$

electrolyte volume in the anode, cathode, and separator (i) are, respectively

$$v_e^i = a_t L^i\left(\varepsilon_l^i + \varepsilon_p^i\right) \tag{22}$$

To calculate the molar flux from the anode or to the cathode, it is necessary to express intermediate molar fluxes to and from the separator, taking into account concentrations at the boundary between separator and compartments, as shown in Figure 3. In this article, each half compartment is considered as the length for diffusion. Hence, for the anode

$$N_{diff}^A = D_{eff}^A \frac{\left(C_e^A - C_e^{A,S}\right)}{L^A/2} a_{tr.e}^A = D_{eff}^S \frac{\left(C_e^{A,S} - C_e^S\right)}{L^S/2} a_{tr.e}^S \tag{23}$$

where effective diffusivity of salt in electrolyte phase in electrodes and the separator is

$$D_{eff}^i = D_{e,o}\left(\varepsilon_l^i + \varepsilon_p^i\right)^{\gamma_{D,i}} \tag{24}$$

It should be noted that flux areas are different in Eq. 23. From this equation, it follows

$$N_{diff}^A = k_l^A\left(C_e^A - C_e^S\right)a_{tr.e}^A \tag{25}$$

and

$$N_{diff}^C = k_l^C\left(C_e^S - C_e^C\right)a_{tr.e}^C \tag{26}$$

being

$$\frac{1}{k_l^i} = \frac{L^i/2}{D_{eff}^i} + \frac{L^S/2}{D_{eff}^S}\frac{\left(\varepsilon_l^i + \varepsilon_p^i\right)}{\left(\varepsilon_l^S + \varepsilon_p^S\right)} \tag{27}$$

where $k_l^A$ and $k_l^C$ can be considered as a global mass-transfer coefficient between anode and separator and separator and cathode.

Combining Eqs. 25 and 26 with (18)–(20)

$$\frac{dC_e^A}{dt} = j^A\left(1-t_+^o\right)\frac{a_{e/s}^A}{v_e^A} - k_l^A\left(C_e^A - C_e^S\right)\frac{a_{tr.e}^A}{v_e^A} \tag{28}$$

$$\frac{dC_e^C}{dt} = -j^C\left(1-t_+^o\right)\frac{a_{e/s}^C}{v_e^C} + k_l^C\left(C_e^S - C_e^C\right)\frac{a_{tr.e}^C}{v_e^C} \tag{29}$$

$$\frac{dC_e^S}{dt} = k_l^A\left(C_e^A - C_e^S\right)\frac{a_{tr.e}^A}{v_e^S} - k_l^C\left(C_e^S - C_e^C\right)\frac{a_{tr.e}^C}{v_e^S} \tag{30}$$

It can be observed that these equations satisfy the global condition

$$\sum v_e^i \frac{dC_e^i}{dt} = 0 \tag{31}$$

## Mass Balances in Particle Electrodes

Solid volume, where reactions occur, both in the anode and cathode can be expressed by means of its corresponding solid fractions

$$v_s^i = a_t\ L^i\ \varepsilon_s^i \tag{32}$$

Mass balances for lithium in the solid phase electrodes take into account the internal diffusion inside particles, and the electrochemical reaction on the surface. Internal concentration distribution in spherical particles depends on time and radius. In this article, particle radius discretization and time discretization will be considered. Figure 4 shows a simplified diagram of lithium distribution for a given time in anodic and cathodic particles, considering one internal division as a discretization scheme. A similar analysis can be made taking into account particles without division (no discetization) but considering internal diffusion; and conversely, considering

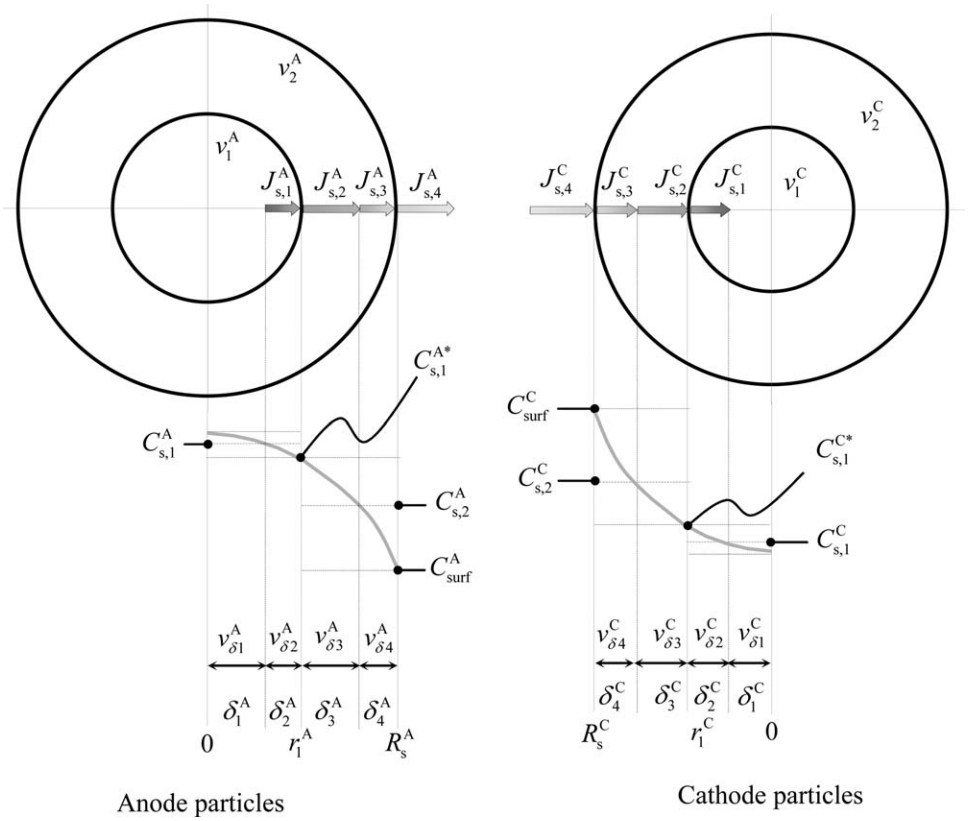


**Figure 4. Li distribution on solid phase, one division on particles.**

two or more divisions, thus increasing the level of discretization and accuracy in the solution.

Similarly to what is considered in the electrolyte phase, local concentration takes the value of the average concentration in a point corresponding to the middle volume of the domain.

The discretization methodology is developed in the following equations for the case shown in Figure 4 that corresponds to only one division of the particle, and can be easily extended to the simplest case without divisions or to more complex cases of several divisions.

The model considers equal volumes for each subdivision. Distances where diffusion occurs are modeled based on the previous assumption, that is, between the middle volume point and the surface of the domain. Mass balances for lithium in anode particles are derived from the previous assumptions

$$v_{s,1}^{A}\frac{dC_{s,1}^{A}}{dt}=-D_{s}^{A}\frac{\left(C_{s,1}^{A}-C_{s,2}^{A}\right)}{\left(\delta_{2}^{A}+\delta_{3}^{A}\right)}a_{1}^{A} \tag{33}$$

$$v_{s,2}^{A}\frac{dC_{s,2}^{A}}{dt}=D_{s}^{A}\frac{\left(C_{s,1}^{A}-C_{s,2}^{A}\right)}{\left(\delta_{2}^{A}+\delta_{3}^{A}\right)}a_{1}^{A}-j^{A}a_{2}^{A} \tag{34}$$

Surface lithium concentration is computed and its value used for calculating the open circuit potential, Eqs. [B-1] and [B-2] from Ref. 8, and the overpotential due to electrochemical reaction (Eq. 15). $C_{surf}^{A}$ is obtained from the following equation

$$C_{surf}^{A}(t)=C_{s,2}^{A}(t)-j^{A}\frac{\delta_{4}^{A}}{D_{s}^{A}} \tag{35}$$

where $\delta_{j}^{i}$ are diffusion distances, calculated taking into account equal volume. A similar analysis can be made for the cathode. Nomenclatures of the above equations are those in Figure 4.

## Determination of a Simple and Accurate Model

The equation system above developed can be resolved numerically. However, as the aim of this work is to obtain a simple and accurate method for calculating all involved variables, different simplifications will be considered and their results will be compared. The set of simplifications that best suits the purposes of the article will be later used for comparison between models and experimental values.

Table 3 provides an overview of the analyzed simplifications or hypothesis. Columns indicate simplifications on the electrolyte phase concentration, and rows indicate the hypothesis applied to electrode particles.

In the first column, salt concentration in electrolyte in the separator is considered constant, and in the second column this concentration is considered variable. As regards rows, the first one considers that electrode particles were not discretized (reaction occurs only on the surface and diffusion is internal). The second row considers that discretization of particles was performed taking into account one division in the particles. And, the third line considers two divisions in

**Table 3. Overview of the Analyzed Models**

| | Electrolyte | |
|---|---|---|
| Particle | $\frac{dC_{e}^{S}}{dt}=0$ | $\frac{dC_{e}^{S}}{dt}\neq 0$ |
| No division | $M_{00}$ | $M_{01}$ |
| One division | $M_{10}$ | $M_{11}$ |
| Two divisions | $M_{20}$ | $M_{21}$ |

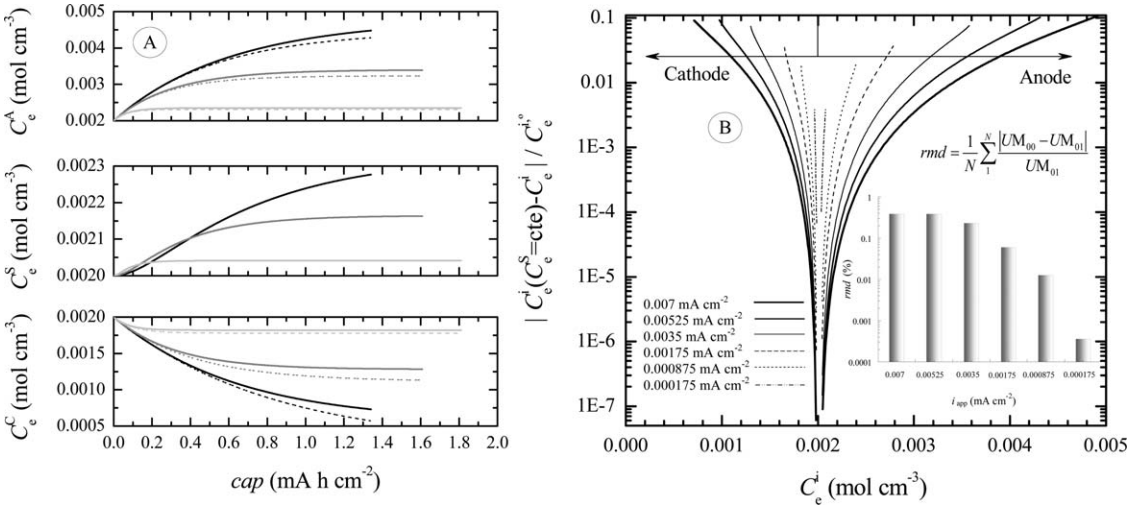


**Figure 5. (A) Electrolyte concentration. No internal division on particles. Comparison between $M_{00}$ and $M_{01}$. Solid line: $M_{01}$. Dot line: $M_{00}$. Black: 0.007 mA cm$^{-2}$. Gray: 0.0035 mA cm$^{-2}$. Ligth Gray: 0.000875 mA cm$^{-2}$. (B) Relative error of salt concentration, between $M_{00}$ and $M_{01}$. Mean relative deviation of cell potential between $M_{00}$ and $M_{01}$.**

particles. So, three sets of hypotheses may be considered by each column in Table 3. Constant concentration in the separator: (1) no division ($M_{00}$); (2) one division ($M_{10}$); (3) two divisions ($M_{20}$). Considering that the separator has variable concentration: (1) no division ($M_{01}$); (2) one division ($M_{11}$); (3) two divisions ($M_{21}$). See Table 3 for more details.

## Comparison Between $M_{00}$ and $M_{01}$

Figure 5A shows salt concentration in electrolyte phase of a generic Cell 1, as a time function for different values of the applied current. Dot line curves correspond to $M_{00}$ whereas solid line corresponds to model $M_{01}$. In Figure 5B, it can be seen the relative error between the salt concentrations, as a function of the salt concentration calculated with model $M_{01}$. In the insert of Figure 5B, it can be seen the variation of the mean relative deviation (variable defined in the same figure) of the potential of the battery in terms of the applied currents. As noted, this parameter does not exceed 1% in the worst case, for the largest current used. Salt concentrations vary up to 100% or more in anode and cathode compartment, while salt concentration in separator varies only up to 10% in cases of high currents. As expected, the higher the applied current the broader the difference between initial and final concentration. However, even the maximum difference is negligible. It can be noted that concentrations predicted from $M_{00}$ are lower than those from $M_{01}$. This effect can be explained taking into account that the assumption of $M_{00}$ did not fulfill the condition given by Eq. 31. Total salt mass changes over time in $M_{00}$, introducing an approximation error. Also, it is clear that for a constant current, the difference between predictions of $M_{00}$ and $M_{01}$ are negligible. Cell potential has been calculated for both models. Maximum potential differences between the values obtained from both models occur close to endpoints, and are lower than 0.03 V.

## Analytical Solution of Salt Concentration in Electrolyte

In this way, we conclude that appropriate potential values are obtained using the simplifying assumption of constant salt concentration in electrolyte separator.

Thus, salt mass balances in the anodic and cathodic electrolytes, Eqs. 28 and 29, can be analytically solved, yielding

$$C_e^A = C_e^{A,0}\exp\left(-k_l^A\frac{a_{tr.e}^A}{v_e^A}t\right)+\left[\frac{j^A\left(1-t_+^o\right)}{k_l^A}\frac{a_{e/s}^A}{a_{tr.e}^A}+C_e^S\right]\times\left[1-\exp\left(-k_l^A\frac{a_{tr.e}^A}{v_e^A}t\right)\right] \quad (36)$$

$$C_e^C = C_e^{C,0}\exp\left(-k_l^C\frac{a_{tr.e}^C}{v_e^C}t\right)+\left[-\frac{j^C\left(1-t_+^o\right)}{k_l^C}\frac{a_{e/s}^C}{a_{tr.e}^C}+C_e^S\right]\times\left[1-\exp\left(-k_l^C\frac{a_{tr.e}^C}{v_e^C}t\right)\right] \quad (37)$$

In the cases studied in these sections, it is considered that the cell discharge is performed by taking appropriate care so as to ensure that initial salt concentration values are equal for all compartments. In this way, Eqs. 36 and 37 can be rewritten in an even simpler way, considering the above equations

$$C_e^{i,0} = C_e^S \quad (38)$$

## Comparison Between $M_{00}$ and $M_{10}$

Cell potentials were compared for both models and for a wide current range. Differences among models appear only for the highest currents. Prediction of final discharge times are almost the same. Maximal relative difference in cell potential occurs at high currents and at initial times and are lower than 4%. At times corresponding to 30% of cell capacity, cell potentials are the same for both models.

## Comparison Between $M_{10}$ and $M_{20}$

Cell potentials were compared for both models in the same way as in the previous case. The differences in cell potentials at the beginning of discharge disappear. Final times predicted by both models are the same. Therefore, model accuracy for cell potential prediction is not improved

by increasing the number of particle divisons. Hence, it can be concluded that model $M_{10}$ is accurate enough for the purpose of this article.

## Analytical Solution of Particle Concentration

The model considering only one particle division can be analytically solved. The following equations must be considered. Average particle concentration is defined from

$$v_s^i \overline{C_s^i} = v_{s,1}^i C_{s,1}^i + v_{s,2}^i C_{s,2}^i \tag{39}$$

and temporal changes of the average concentration

$$v_s^i \frac{d\overline{C_s^i}}{dt} = \mp j^i a_2^i \tag{40}$$

being $(-)$ for i = anode and $(+)$ for i = cathode. Upon algebraic manipulation and applying the method of integrating factor

$$C_{s,2}^i = C_{s,2}^{i,0} \mp j^i \frac{a_2^i}{v_s^i} \left[ t + \frac{1 - \exp\left( - \frac{4D_s^i}{(\delta_2^i + \delta_3^i)} \frac{a_1^i}{v_s^i} \, t \right)}{\frac{4D_s^i}{(\delta_2^i + \delta_3^i)} \frac{a_1^i}{v_s^i}} \right] \tag{41}$$

$$C_{s,1}^i = C_{s,1}^{i,0} \mp j^i \frac{a_2^i}{v_s^i} \left[ t - \frac{1 - \exp\left( - \frac{4D_s^i}{(\delta_2^i + \delta_3^i)} \frac{a_1^i}{v_s^i} \, t \right)}{\frac{4D_s^i}{(\delta_2^i + \delta_3^i)} \frac{a_1^i}{v_s^i}} \right] \tag{42}$$

The exponential term in Eqs. 41 and 42 is important only for high values of discharge current at the beginning of the discharge. At the end of the discharge process, the exponential term reaches values lower than $1.10^{-3}$. Thus, the exponential term can be removed, giving rise to "Simplified $M_{01}$"

$$1 - \exp\left( -4 \frac{D_s^i}{(\delta_2^i + \delta_3^i)} \frac{a_1^i}{v_s^i} \, t \right) \cong 1 \tag{43}$$

With this additional simplification, cell potentials remain almost unchanged. Differences lower than 4% can be computed at the beginning of discharge.

"Simplified $M_{01}$" model is composed of a set of algebraic equations that can be alternatively used to predict discharge processes or to correlate the operating parameters of a lithium ion battery.

Summarizing, the assumption of constant salt concentration in the separator plus the diffusion model in particles with only one particle division result appropriate for cell potential predictions in the whole range of analyzed currents. With these assumptions, model $M_{10}$ was analytically solved. In this way, it has succeeded in transforming the original system of differential algebraic equations into a system of independent algebraic equations composed of: one equation for salt concentration in each electrode (Eqs. 36 and 37), three equations for anodic particles, and three for cathodic particles (Eqs. 35, 41, and 42). $M_{10}$ can be further simplified by eliminating exponential time terms, giving rise to "Simplified $M_{10}$" model.

## Model Validation

A comparison between theoretical predictions obtained from the analytical model $M_{10}$, theoretical predictions according to the simplified $M_{10}$ analytical model, and the experimental points for Cell 1 and Cell 2 from Ref. 8 is depicted in Figures 6A, B. Note that most of the parameters

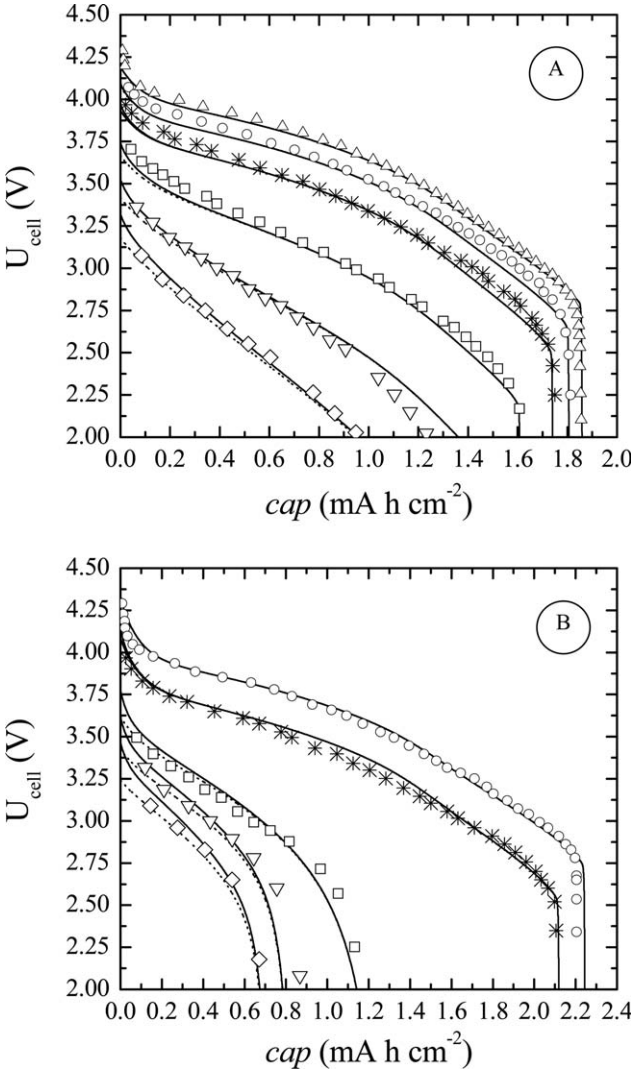


**Figure 6. Comparison with experimental point, according to Ref. 8.**

**Solid line: analytical model. Dot line: simplified analytical model. Symbols: experimental points. Units current discharges: mA cm$^{-2}$. Cell 1 (A). (◇): 0.007. (▽): 0.00525. (□): 0.0035. (*): 0.00175. (○): 0.000875. (△): 0.000175. Cell 2 (B). (◇): 0.010416. (▽): 0.008333. (□): 0.00625. (*): 0.002084. (○): 0.0004167.**

were taken from the reference article and only $\gamma_\kappa$ and $\gamma_D$ were set to 3 instead 3.3 in order to approximate the experimental values for Cell 1. However, salt diffusion coefficient and effective conductivity exponents were adjusted at other values than those from the reference for Cell 2. As it can be seen, predictions of the analytical model have a very good agreement with the experimental points. It should be mentioned that other different parameters sets can be used given a very good agreement between experimental and theoretical results. Furthermore, electrolyte discretization and slightly different cell potential calculation were implemented obtaining the same good approximations.

Model validation was performed only for discharge experiments. As the authors mentioned in the reference article, the values obtained for cell potential in charge processes were subjected to uncertainty because of the effect of previous discharge at moderate currents. It was not possible to reproduce the charge curves without modifying model parameters.

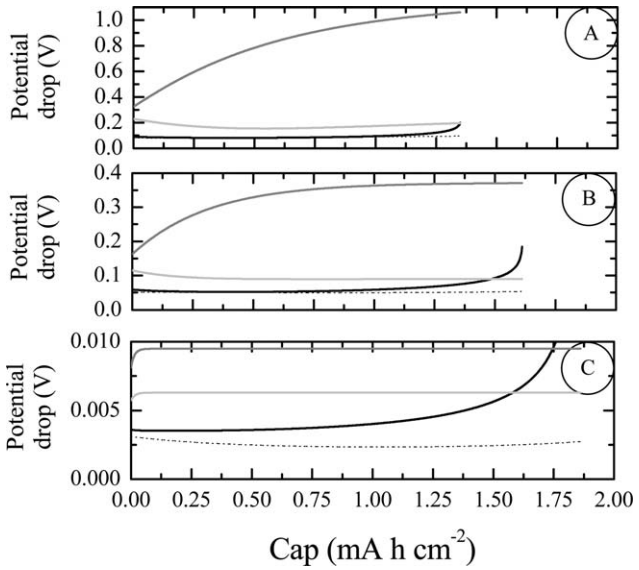


**Figure 7. Potential of the different phases on the battery.**

**Cell 1. (A) 0.007 mA cm$^{-2}$. (B) 0.0035 mA cm$^{-2}$. (C) 0.000175 mA cm$^{-2}$. Gray: $\Delta\phi_e^A$. Light gray: $\Delta\phi_e^C$. Black: $\eta^A$. Dash: $\eta^C$.**

Figure 7 shows the most important potential drop values for each phases of the battery for three applied current values. As it can be seen, regardless of the applied current, the potential drop in electrolyte of the anode followed by that in electrolyte of the cathode are the most important. However, the potential drop which determines the final abrupt potential collapse for this battery is the anode overpotential corresponding to electrochemical reaction. This fact is due to the lithium exhaustion in the anode particles which produces exchange current, $j0^A$ drops to zero and consequently $\eta^A$ tends to infinity. Energy efficiency in batteries is determined by potential drops during the whole discharge process. Conversely, capacity of a battery is determined by the final potential fall. Hence, energy efficiency and capacity of batteries could be associated with different limiting phenomena as shown in the previous case, where, energy efficiency will be related to electrolyte potential drop, whereas capacity will be related to anode particle exhaustion. In the next section, discharge time and capacity usage will be investigated.

## Discharge Time and Capacity Usage Estimation

The capacity of cells operating at constant current are computed when the potential falls to zero. These final capacities depend on battery design as well as on the applied current as can be derived from Figure 6. The limiting processes that take place in the discharge are: lithium consumption from anode, lithium intercalation in cathode, and salt concentration depletion in the cathode. The processes here considered are only related to mass balances. Other limiting conditions such as high potential drops could be possible, but they are not analyzed here. Furthermore, in the model presented in this article, mass balances can be calculated independently of the cell potential. Hence, while some concentrations remain greater than zero, others reached zero or negative values in previous times.

The previously developed equation system is composed of analytical equations predicting lithium salt concentration in the electrolyte of electrodes and lithium concentration in particles. Analyzing each one of these equations in isolation, it can be inferred that the final discharge point is mainly related to the following conditions:

a. salt concentration in cathode electrolyte is zero;
b. surface particle lithium concentration of the anode reaches zero;
c. surface particle lithium concentration of the cathode reaches its maximum value.

One or more of these conditions can determine the final operating time of the battery.

By equating Eq. 17 to zero, final discharge time can be obtained. This equation, however, can be solved only numerically, and consequently no physical information would be derived.

Considering that, at the beginning of discharge, all salt concentrations in the compartments are equal, and the separator concentration is constant, from Eq. 37 and considering $C_e^C$ is set to zero, the corresponding value for time is obtained

$$t_e^C = -\frac{1}{k_l^C}\frac{v_e^C}{a_{tr.e}^C}\ln\left[1 - C_e^{C,0}\frac{k_l^C}{j^C(1-t_+^o)}\frac{a_{tr.e}^C}{a_{e/s}^C}\right] \tag{44}$$

By equating the surface concentration to zero for anode particles in Eqs. 35 and 41, the corresponding time is obtained

$$t_s^A = \frac{C_{s,2}^{A,0}}{j^A}\frac{v_s^A}{a_2^A} - \frac{1}{D_s^A}\frac{v_s^A}{a_2^A}\left[\frac{(\delta_2^A+\delta_3^A)}{4}\frac{a_2^A}{a_1^A} + \delta_4^A\right] \tag{45}$$

By performing the same analysis with the surface lithium concentration in cathode particles and solving for time

$$t_s^C = \frac{C_{max}^C - C_{s,2}^{C,0}}{j^C}\frac{v_s^C}{a_2^C} - \frac{1}{D_s^C}\frac{v_s^C}{a_2^C}\left[\frac{(\delta_2^C+\delta_3^C)}{4}\frac{a_2^C}{a_1^C} + \delta_4^C\right] \tag{46}$$

The second term in the argument of the logarithm in Eq. 44 is greater than unity for all values of the current tested for Cell 1. This term is 1.13 for the highest current, 0.007 mA h cm$^{-2}$, and 45.20 for the case of the lowest current, 0.000175 mA h cm$^{-2}$. Salt concentration of the cathodic compartment will never be zero and, therefore, concentration in the cathode compartment does not affect the battery operation for this battery design and operating conditions. Equation 44 provides a solution only for currents greater than 0.00791 mA h cm$^{-2}$.

Table 4 shows in the first column the applied current. In the second column the time in which cell potential fall to zero computed by model $M_{11}$. In third and fourth column the times at which electrolyte salt concentration in cathode fall to zero, computed by $M_{11}$ and Simplified $M_{10}$ respectively. In fifth and sixth the times at which lithium concentration in solid particles in anode fall to zero, computed by $M_{11}$ and Simplified $M_{10}$ respectively. And finally in columns seventh and eighth the times at which lithium concentration in solid particles in cathode reach the maximum, computed by $M_{11}$ and Simplified $M_{10}$ respectively. Results from Simplified $M_{10}$ agree with the results from $M_{11}$. Exhausting lithium in solid anode particles limit time discharge for currents lower than 0.01 mA cm$^{-2}$ for Cell 1. Cell potential drop to zero for the remaining cases for Cell 1 and Cell 2 before the three conditions are accomplished. In these cases, cell potential drops to zero at values of time very close to those computed by conditions of either a) cathode electrolyte salt exhaustion, or b) anode solid lithium depletion.

Table 4. Comparison Between Discharge Time, for Two Typical Cells

| $i_{app}$ (mA cm$^{-2}$) | Discharge Time (s). $M_{1,1}$ | $t_e^C$ (s) - Cap (mA h cm$^{-2}$) | | $t_s^A$ (s) - Cap (mA h cm$^{-2}$) | | $t_s^C$ (s) - Cap (mA h cm$^{-2}$) | |
|---|---|---|---|---|---|---|---|
| | | $M_{1,1}$ | Simplified $M_{1,0}$ Eq. 44 | $M_{1,1}$ | Simplified $M_{1,0}$ Eq. 45 | $M_{1,1}$ | Simplified $M_{1,0}$ Eq. 46 |
| **A: Cell 1** | | | | | | | |
| 0.000175 | 38,278 | Nonactive | Nonactive | 38,278 – 1.86 | 38,345 – 1.86 | 54,040 – 2.63 | 53,973 – 2.62 |
| 0.000875 | 7438 | Nonactive | Nonactive | 7438 – 1.81 | 7453 – 1.81 | 10,755 – 2.61 | 10,756 – 2.64 |
| 0.00175 | 3582 | Nonactive | Nonactive | 3582 – 1.74 | 3592 – 1.75 | 5355 – 2.60 | 5354 – 2.60 |
| 0.0035 | 1656 | Nonactive | Nonactive | 1656 – 1.61 | 1661 – 1.61 | 2652 – 2.58 | 2652 – 2.58 |
| 0.00525 | 1014 | Nonactive | Nonactive | 1014 – 1.48 | 1017 – 1.48 | 1752 – 2.56 | 1752 – 2.56 |
| 0.007 | 693 | Nonactive | Nonactive | 693 – 1.35 | 696 – 1.35 | 1302 – 2.53 | 1302 – 2.53 |
| 0.008 | 575 | Nonactive | 1885 – 4.19 | 575 – 1.28 | 575 – 1.28 | 1133 – 2.52 | 1133 – 2.52 |
| 0.01 | 412 | 1154 – 3.2 | 657 – 1.83 | 413 – 1.15 | 406 – 1.13 | 897 – 2.49 | 897 – 2.49 |
| 0.015 | 185 | 340 – 1.42 | 315 – 1.31 | 214 – 0.89 | 181 – 0.75 | 582 – 2.42 | 582 – 2.42 |
| 0.02 | 85 | 218 – 1.21 | 211 – 1.17 | 129 – 0.72 | 68 – 0.38 | 424 – 2.36 | 424 – 2.36 |
| **B: Cell 2** | | | | | | | |
| 0.0004167 | 19,401 | Nonactive | Nonactive | 19,438 – 2.25 | 19,441 – 2.25 | 25,233 – 2.92 | 25,248 – 2.92 |
| 0.002084 | 3662 | Nonactive | Nonactive | 3666- 2.12 | 3671 – 2.13 | 5002 – 2.90 | 5009 – 2.90 |
| 0.00625 | 886 | 978 – 1.7 | 760 – 1.32 | 1042 – 1.81 | 1044 – 1.81 | 1633 – 2.83 | 1638 – 2.84 |
| 0.00833 | 369 | 378 – 0.87 | 365 – 0.68 | 715 – 1.66 | 716 – 1.66 | 1213 – 2.81 | 1217 – 2.82 |
| 0.010416 | 250 | 255 – 0.74 | 251 – 0.73 | 521 – 1.51 | 519 – 1.50 | 960 – 2.78 | 963 – 2.79 |
| 0.015 | 149 | 152 – 0.63 | 152 – 0.63 | 296 – 1.23 | 278 – 1.16 | 651 – 2.71 | 654 – 2.73 |
| 0.02 | 104 | 106 – 0.59 | 107 – 0.59 | 182 – 1.01 | 141 – 0.78 | 476 – 2.64 | 478 – 2.66 |

As it can be seen, for these geometric designs and operating conditions, discharge time of the battery is only conditioned by lithium consumption in the anode particles at low currents. However, the situation is quite different at high current values, where either salt depletion in the cathode compartment or potential drops inside the battery limit the final discharge time and capacity.

Considering low currents at which Eq. 45 provides the actual value of discharge final time, the final capacity results

$$\text{cap}=t_s^A\ i_{app}=C_{s,2}^{A,0}L^A F\varepsilon_s^A-\frac{R_s^A}{3\ D_s^A}\ i_{app}\left[\frac{\left(\delta_2^A+\delta_3^A\right)}{4\ 2^{-2/3}}+\delta_4^A\right] \quad (47)$$

Equation 47 indicates that the capacity delivered by the battery involves the sum of two terms: the first one is positive and depends only on design variables, whereas the second one is negative and depends on the applied current, anodic particle radius, and diffusion coefficient in the solid particle. The first term can be considered as "initial capacity" and the second term can be considered as "lost capacity." If design variables are modified, that is, $L^A$, $R_s^A$, $C_{s,2}^{A,0}$, and so forth, the set of Eqs. 44, 45, and 46 should be analyzed in order to determine the process bottleneck. In Figure 8, lost capacity is plotted as a function of discharge applied current and dimensionless electrodes particle sizes for Cell 1. Anodic lost capacity is greater than cathodic lost capacity for the whole range of currents and particle sizes. The term in square brackets in Eq. 47 corresponds to $0.44\ R_s^A$, hence the term $D_s^A/\left(0.44\ R_s^A\right)$ can be interpreted as a mass-transfer coefficient. This means that diffusion length for the average lithium concentration in the particle is approximately half the particle radius. A characteristic number for lost capacity is related to the time associated with diffusion in the particle. From Eq. 45 or 46, time reduction due to internal particle diffusion is approximately $\left(R_s^A\right)^2/\left(6\ D_s^A\right)$ [s] that corresponds to a lost capacity independent of the applied current.

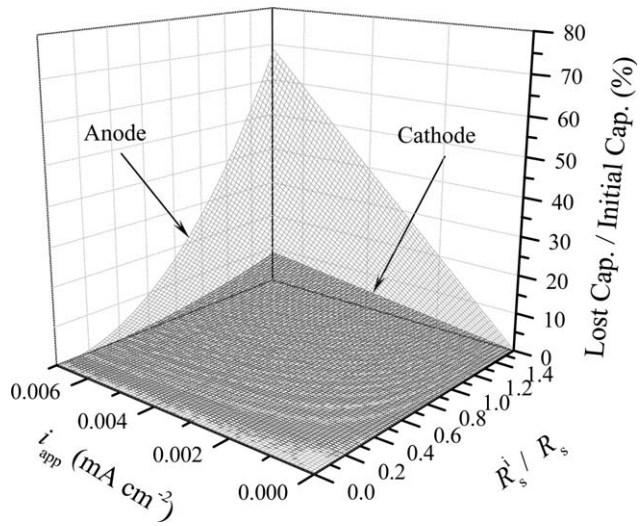


**Figure 8. Relation between lost capacity and initial capacity vs. applied current and dimensionless anodic and cathodic particle radius.**

## Relaxation Time Estimation

Relaxation processes were previously addressed in Ref. 23. As pointed out by the authors, charge and discharge cyclic processes are strongly affected by relaxation processes. Diffusion in electrolytes and particles are extreme low rate phenomena and its extent will be investigated here. The same algebraic equations previously derived and used for capacity estimations can be applied to compute relaxation times. In fact, diffusion equations (Eqs. 33, 34, and 39) are used with the electrochemical reaction rate term set to zero, as relaxation occurs at zero applied current. Considering this and assuming that the analyzed cell concentrations are restored up to 99% of the final equilibrium value, an equation can be obtained for a quick prediction of relaxation times in anodic particles

$$t_{s,R}^A=-\frac{\left(\delta_2^A+\delta_3^A\right)}{D_s^A}\frac{v_s^A}{a_1^A}\ln\left[\frac{\left(1.01\ \overline{C_s^A}-\overline{C_s^A}\right)}{\left(C_{s,1}^A-\overline{C_s^A}\right)}\right] \quad (48)$$

A similar analysis can be made for the other compartments. The concentration profiles for anodic particles (inner and outer) of Cell 1 for two different moderate applied discharge currents are compared in Figure 9. 1000 s after the beginning of the discharge, the battery is switched off. As a

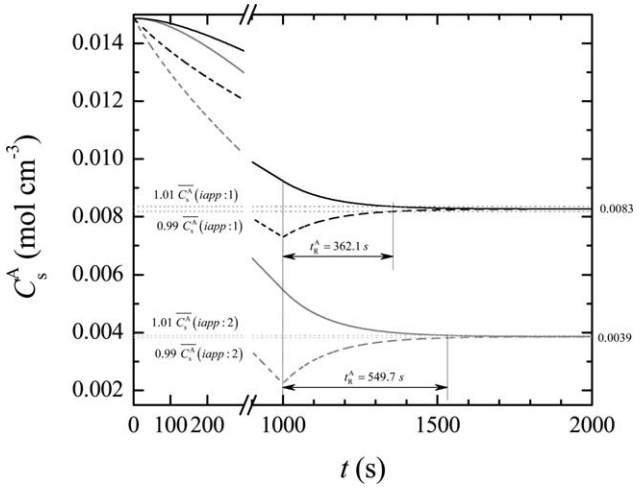


**Figure 9. Relaxation time in anodic particles.**

**Solid: inner. Dash: outer. Black line: particle concentration at $i_{app} = 0.003$ mA cm$^{-2}$. Gray lines: particle concentration at $i_{app} = 0.005$ mA cm$^{-2}$.**

consequence, concentrations tend to a final equilibrium value given by Eq. 39. In both curves, relaxation time calculated with Eq. 48 is shown. As previously mentioned, relaxation times are of the same magnitude order as discharge times.

## Cyclic Processes

Cyclic processes studied here are composed of only one discharge and only one charge of a given battery in a given time period, as it is shown in Figure 10. Different charge schedules are possible in order to re-establish the initial condition of the battery and reinitiate the cycle. Mathematical conditions must be imposed on the model equations. Final salt and lithium concentration in all compartments must be equal to the initial ones. Such cycles that accomplish those conditions are considered to be in steady state. The following conditions are known: cycle time, battery design, discharge applied current, and time.

Under this setting, the cycle energy efficiency should be optimized by finding the charge current and time. In the case here studied, it is assumed that both discharge and charge are performed at constant current. Energy efficiency is measured as the quotient between energy delivered by the cell in discharge process and the energy consumed in the charge one. Energy loss is related to potential drop along time in each process. By modifying charge schedule, it is possible to improve efficiency in the charge section.

Reversible work can be computed for charge and discharge processes independently. In fact, assuming no potential drop inside the battery along each process, the product of open circuit potential and applied current can be integrated along time in order to compute reversible work. Cell 1 of 1 cm$^2$ and current discharge of 0.03 mA is considered.

Current profiles for discharge and charge are shown in Figure 10A. Cell potential is shown in part B of the same figure. Relaxation processes can be observed and the higher the charge current the higher the peak cell potential and the lower the charge times. Concentrations profiles in electrolyte and solid particles are depicted in parts C and D for charge at 0.015 mA. In the same way, relaxation times in electrolyte and solid can be observed.

As the process is cyclic, charge and discharge reversible work show the same value: 19 mW s. In contrast, real work in discharge at a current of 0.03 mA results in 16.38 mW s

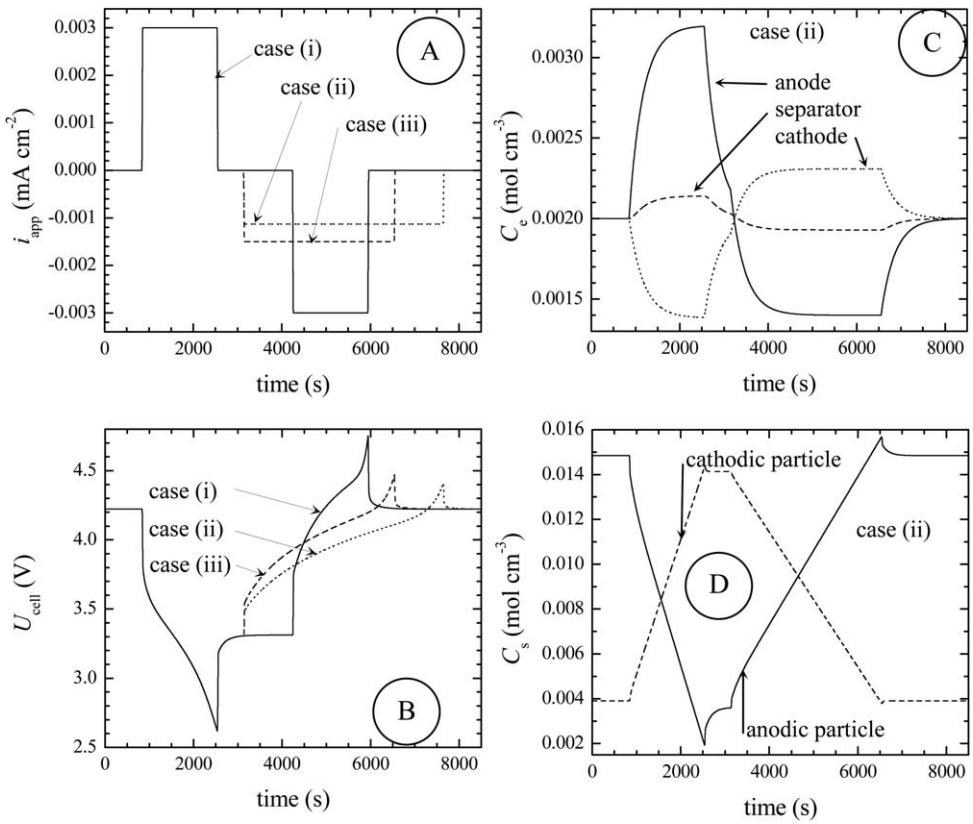


**Figure 10. Discharge and charge cycles at constant applied current.**

**Efficiency and COP studies.**

providing a 86.2% efficiency in discharge when compared to the reversible process. At charge current of 0.03 mA, real work results 21.69 mW s and coefficient of performance (COP) results 87.6%. At charge current of 0.015 mA, real work results 20.49 and COP 92.7%, and finally at 0.01132 mA, real work results 20.21 and COP 94%. It should be noted that efficiencies are nonsymmetric although discharge and charge were carried out at the same current in the case of 0.03 mA. This is due to electrochemical kinetics.

## Numerical Aspects

For constant current and simple discharge or charge processes, the model was developed and solved in Excel and in General Algebraic Modeling System (GAMS).[26] Differential algebraic equations of $M_{11}$ were solved using different numerical approximations such as Euler, Runge Kutta, Adam Bradford, and trapezoidal methods. Grid size of 1000 nodes was sufficient for Euler method for all the cases. CPU times were lower than 1 s in Excel and lower than 2 s in GAMS when simulating simple discharge or charge processes. In the web page,[27] a simulator written in Excel is available for download. In this application, it is possible to change the applied current, geometric design parameters, operating parameters, and volume fraction in order to test the model response.

For cyclic processes satisfying the same concentration values at initial and final cycle point, the model was developed in GAMS. In this case, CPU times were lower than 30 s. Nonequilibrium conditions can be considered at the initial and final point of a cycle; that is, concentration gradients could be observed along the whole cycle.

## Conclusions

1. A simplified phenomenological model for cell discharge and charge was presented. The approach is based on: average computation of current densities, concentrations, reaction rates, and diffusion fluxes.
2. This mathematical model generates a system of ordinary differential equations through the expression of mass balances of salt and lithium in the compartments and particles. Particle discretizations provide accurate enough solutions resorting to only one domain division. Electrolyte discretization is not necessary. Increasing discretization did not change simulation results.
3. Considering the concentration in the separator remains constant and particles are discretized in two divisions, the system of ordinary differential equation was analytically integrated. This analytical model was able to predict, with a very good degree of agreement, discharge experiments involving two different batteries from the literature, and its resolution took less than 1 s. Parameters were taken from the literature and no additional internal resistances were necessary to adjust experimental values.
4. This analytical model was simplified even further, and this simplification allowed predicting final times of battery discharges and recharges. Also, the agreement between these predictions and the prediction from the original model (1) was very good. Initial capacity and lost capacity were defined from a simple set of cell design and operating parameters.
5. The model allows calculating discharge and recharge cycles of lithium-ion batteries, in order to study the behavior of the most important process variables, and to identify the duration of these batteries relaxation times.
6. For a specific cell design, energy efficiency in cyclic process was dominated by potential drop in the anodic electrolyte whereas final cell capacity was dominated by lithium exhaustion in anode particles.
7. Future works based on the models and the results arrived to in this article will address optimal operation conditions for charge and discharge cycles.

## Acknowledgment

The authors acknowledge financial support provided by Consejo Nacional de Investigaciones Científicas y Técnicas (CONICET), Agencia Nacional de Promoción Científica y Tecnológica (ANPCyT) of Argentina, and Universidad Nacional del Litoral (UNL).

## Notation

$a$ = area, $cm^2$
$\bar{C}$ = average concentration, mol $cm^{-3}$
cap = capacity, mA h $cm^{-2}$
$C$ = concentration, mol $cm^{-3}$
$i$ = current density, mA $cm^{-2}$
$D$ = diffusion coefficient, $cm^2$ $s^{-1}$
$F$ = Faraday constant, 96,486 C $mol^{-1}$
$j$ = electrochemical reaction rate, mol $s^{-1}$ $cm^{-2}$
$j0$ = exchange current density, A $cm^{-2}$
$L$ = length, cm
$N$ = molar flux per unit area, mol $cm^{-2}$ $s^{-1}$
$J$ = molar flux, mol $s^{-1}$
$U$ = potential, V
$t$ = time, s
$v$ = volume, $cm^3$

### *Specials and Greek*

$t_+^o$ = transport number
$f_\pm$ = molar activity coefficient of the salt
$\varepsilon$ = volume fraction
$\kappa$ = electrolyte conductivity, S $cm^{-1}$
$\Delta\phi$ = potential drop, V
$\sigma$ = solid conductivity, S $cm^{-1}$
$\eta$ = overpotential, V
$k$ = mass-transfer coefficient, cm $s^{-1}$
$\gamma$ = Bruggeman's exponent

### *Subscript*

app = applied
cell = cell
diff = diffusion
e = electrolyte
eff = effective
e/s = electrolyte in contact with solid
f = filler
l = liquid
max = maximum
o = pure
p = polymer
R = relaxation
s = solid
surf = surface
t = transversal
tr.e = transversal area of electrolyte phase
tr.s = transversal area of solid phase

### *Superscript*

A = anode
C = cathode
i = anode, cathode, or separator
S = separator
0 = initial
o = pure

## Literature Cited


1. Tarascon JM, Armand M. Issues and challenges facing rechargeable lithium batteries. *Nature*. 2001;414:359–367.
2. Bashash S, Moura SJ, Forman JC, Fathy HK. Plug-in hybrid electric vehicle charge pattern optimization for energy cost and battery longevity. *J Power Sources*. 2011;196:541–549.
3. Shiau CSN, Kaushal N, Hendrickson CT, Peterson SB, Whitacre JF, Michalek JJ. Optimal plug-in hybrid electric vehicle design and allocation for minimum life cycle cost, petroleum consumption, and greenhouse gas emissions. *J Mech Des*. 2010;132:1–11.
4. Vazquez-Arenas J, Fowler M, Mao X, Chen S. Modeling of combined capacity fade with thermal effects for a cycled $Li_xC_6$-$Li_yMn_2O_4$ cell. *J Power Sources*. 2012;215:28–35.
5. Kumar M, Singh SN, Srivastava SC. Design and control of smart dc microgrid for integration of renewable energy sources. IEEE Power and Energy Society General Meeting. San Diego, CA. 2012:1–7.
6. Darcovich K, Henquin ER, Kenney B, Davidson IJ, Saldanha N, Beausoleil-Morrison I. Higher-capacity lithium ion battery chemistries for improved residential energy storage with micro-cogeneration. *Appl Energy*. 2013;111:853–861.
7. Bashash S, Moura S, Forman J, Fathy H. Plug-in hybrid electric vehicle charge pattern optimization for energy cost and battery longevity. *J Power Sources*. 2011;196:541–549.
8. Doyle M, Newman J, Gozdz AS, Schmutz CN, Tarascon JM. Comparison of modelling predictions with experimental data from plastic lithium ion cell. *J Electrochem Soc*. 1996;143(6):1890–1903.
9. Boovaragavan V, Subramanian VR. A quick and efficient method for consistent initialization of battery models. *Electrochem Commun*. 2007;9:1772–1777.
10. Santhanagopalan S, Guo Q, Ramadass P, White RE. Review of models for predicting the cycling performance of lithium ion batteries. *J Power Sources*. 2006;156:620–628.
11. Dao T-S, Vyasarayani CP, McPhee J. Simplification and order reduction of lithium-ion battery model based on porous-electrode theory. *J Power Sources*. 2012;198:329–337.
12. Subramanian VR, Diwakar VD, Tapriyal D. Efficient macro-micro scale coupled modeling of batteries. *J Electrochem Soc*. 2005; 152(10):A2002–A2008.
13. Smith K, Wang CY. Solid-state diffusion limitations on pulse operation of a lithium ion cell for hybrid electric vehicles. *J Power Sources*. 2006;161:628–639.
14. Boovaragavan V, Harinipriya S, Subramanian VR. Towards real-time (milliseconds) parameter estimation of lithium-ion batteries using reformulated physics-based models. *J Power Sources*. 2008; 183:361–365.
15. Zhang Q, White RE. Comparison of approximate solution methods for the solid phase diffusion equation in a porous electrode model. *J Power Sources*. 2007;165:880–886.
16. Subramanian VR, Ritter JA, White RE. Approximate solutions for galvanostatic discharge of spherical particles I. *Constant diffusion coefficient*. *J Electrochem Soc*. 2001;148(11):E444–E449.
17. Botte GG, Subramanian VR, White RE. Mathematical modeling of secondary lithium batteries. *Electrochim Acta*. 2000;45:2595–2609.
18. Subramanian VR, Boovaragavan V, Ramadesigan V, Arabandi M. Mathematical model reformulation for lithium-ion battery simulations: galvanostatic boundary conditions. *J Electrochem Soc*. 2009; 156(4):A260–A271.
19. Verbrugge M. Three-dimensional temperature and current distribution in a battery module. *AIChE J*. 1995;41(6):1550–1562.
20. Ng J, Dubljevic S. Boundary control synthesis for a lithium-ion battery thermal regulation problem. *AIChE J*. 2013;59(10):3782–3796.
21. Boovaragavan V, Ramadesigan V, Panchagnula MV, Subramanian VR. Continuum representation for simulating discrete events of battery operation. *J Electrochem Soc*. 2010;157(1):A98–A104.
22. Benger R, Wenzl H, Beck HP, Jiang M, Ohms D, Schaedlich G. Electrochemical and thermal modeling of lithium-ion cells for use in HEV or EV application. *World Electr Veh J*. 2009;3:1–10.
23. Erdinc O, Vural B, Uzunoglu M. A dynamic lithium-ion battery model considering the effects of temperature and capacity fading. IEEE 2009 International Conference on Clean Electrical Power. Capri, Italy, 9–11 June 2009, 383–386.
24. Fuller TF, Doyle M, Newman J. Relaxation phenomena in lithium-ion-insertion cells. *J Electrochem Soc*. 1994;141:982–990.
25. Nestle NFEI, Kimmich R. Concentration-dependent diffusion coefficients and sorption isotherms. *Application to ion exchange processes as an example*. *J Phys Chem*. 1996;100(30):12569–12573.
26. Brooke A, Kendrich D, Meeraus A, Raman R. *GAMS Language Guide, RELEASE 2.25, Version 92*. Washington, D.C.:GAMS Development Corporation, 1997.
27. Available at http://www.ingar.santafe-conicet.gov.ar/proyectos/li-ion-batteries/. INGAR - Instituto de Desarrollo y Diseño. Project made by E. R. Henquín and P. A. Aguirre. 2014. Santa Fe, Argentina.


*Manuscript received Apr. 3, 2014, and revision received Aug. 5, 2014.*